Construction and Building Materials 344 (2022) 128085

Contents lists available at ScienceDirect

Construction and Building Materials

journal homepage: www.elsevier.com/locate/conbuildmat

Effect of freeze–thaw cycles on the void topologies and mechanical properties of asphalt

D. Sanfilippo [a], A. Garcia-Hernández [a,*], A. Alexiadis [b], B. Ghiassi [c]

[a] Nottingham Transportation Engineering Centre, Department of Civil Engineering, University of Nottingham, Nottingham NG7 2RD, United Kingdom
[b] School of Chemical Engineering, University of Birmingham B15 2TT, UK
[c] Department of Civil Engineering, University of Birmingham B15 2TT, UK

ARTICLE INFO

Keywords:
Asphalt
Freeze–thaw damage
Mechanical properties
Voids topology
Performance deterioration

ABSTRACT

Frost and thawing damage asphalt in cold climates. Water that enters the pores of asphalt at low temperatures may accelerate its degradation. Water can expand into pores, altering the void content and shape, thus affecting the asphalt's internal structure and fracture properties. We can develop more durable asphalt types if we understand how void topology changes with freeze–thaw cycles. The purpose of this study is to establish a correlation between the mechanical properties of asphalts and the topological properties of voids. To determine their internal structure, various asphalt types representing dense asphalt and asphalt with voids were made and X-rayed before and after each freeze–thaw cycle. We also obtained the mechanical properties of asphalt and correlated them with the void properties. It was found that dense asphalt has the lowest degradation rate in wet conditions characterised by non-connected gaps, which was approximately constant with freeze–thaw cycles; however, dense asphalt was least durable under dry conditions compared with asphalts with more voids. Due to its high water retention rate, asphalt with a 10% void content degraded at an accelerated rate during the initial cycles. As a result of bigger voids, asphalt with a higher pore content plateaued in later cycles due to reduced water retention. This study demonstrates that the internal void topology affects the mechanical properties of asphalt during freeze–thaw cycles. These results can be used to understand changes in asphalt mechanical losses resulting from freeze-thaw cycles and to validate numerical models to perform parametric studies of the asphalt's freeze–thaw degradation.

1. Introduction

Asphalt mixture is a heterogeneous material made of aggregates, mineral filler, and a bituminous binder. It is compacted at temperatures ranging between 135 °C and 155 °C; asphalt mixtures may also include voids, up to more than 20 % of the total asphalt's volume, depending on the gradation and compaction methodology. Asphalt is the most used material to build pavement surfaces. Asphalt undergoes different mechanical loads and environmental conditions during its lifetime, leading to crack and damage and reducing its lifespan [1,2]. In particular, the extreme environmental condition in cold regions with large temperature fluctuations [3] and the water permeation are some of the most harmful deterioration mechanisms that may affect asphalt, leading to thermal stress [4], loss of adhesion at the interface between aggregate and bitumen [5], and loss of cohesion of the binder [6].

The binder is a viscoelastic material at high temperatures, while the aggregates are elastic in all the ambient temperature ranges. Moreover, at low temperatures, the binder is an elastic and brittle material [7]. Several factors influence asphalt's mechanical properties, including its temperature, freeze–thaw cycles, air void content and internal void topology. In addition, the air voids content can increase due to the expansion of water under freeze–thaw actions, increasing asphalt's permeability and, consequently, the risk of freeze–thaw damage [3,8]. If water infiltrates the asphalt, it can freeze and expand, increasing the pressure in the pores, modifying the void content and shape, causing cracks and weakening the asphalt. Cracks may appear, creating new voids that alter the internal void structure [9]. Once the ice melts, water may permeate the cracks; and new freeze–thaw cycles may increase damage, following the same mechanism. Consequently, the stiffness modulus [10], strain energy [10], fracture toughness [11], critical stress [11], splitting strength [12], and maximum flexural tensile strain [12], of asphalt may reduce.

* Corresponding author.
E-mail address: alvaro.garcia@nottingham.ac.uk (A. Garcia-Hernández).

https://doi.org/10.1016/j.conbuildmat.2022.128085
Received 14 January 2022; Received in revised form 18 May 2022; Accepted 7 June 2022
Available online 24 June 2022

Table 1
Asphalt mixture composition.

Size (mm)	Target void content, %		
	3%	9.8%	14%
20	0	23.6	0
14	0	42.4	0
10	58.9	0	63.5
6.3	7.5	9.4	18.9
Dust	18.7	12.3	7.6
Filler	8.4	6.6	4.7
Bitumen	6.5	5.7	5.5
Air void content	3	9.8	14

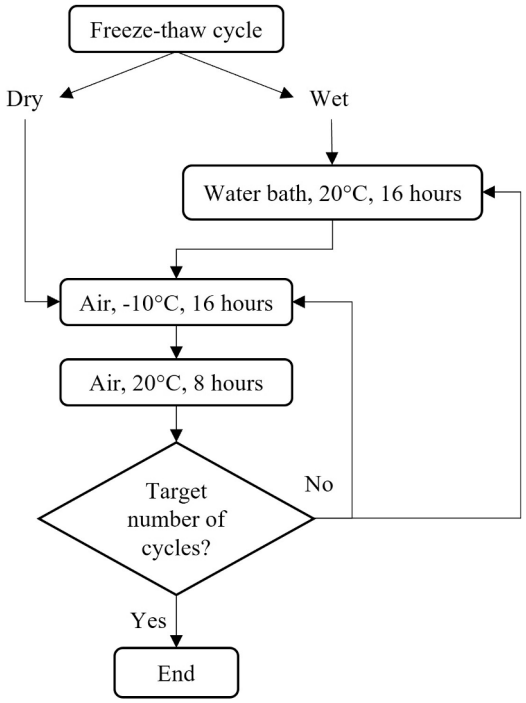

Fig. 1. Steps followed for the freeze–thaw tests of asphalt.

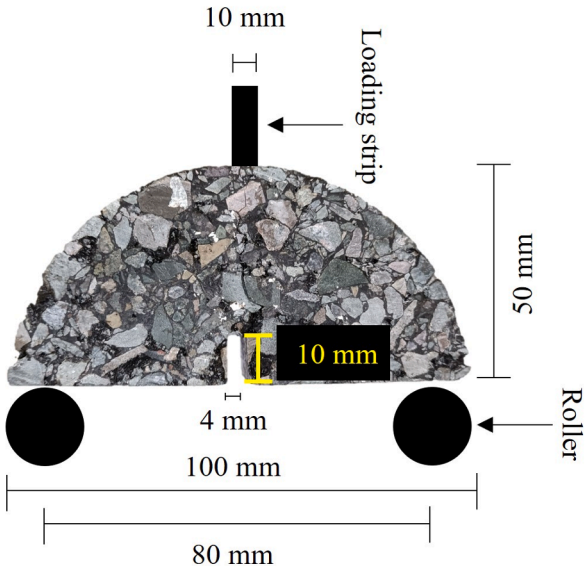

Fig. 2. Semi-circular bending test.

Previous researchers have investigated the influence on mechanical properties of freeze–thaw cycles on asphalt using semi-circular bending and 3-point bending tests at low temperatures. Semi-circular bending is one of the most popular tests to characterise the cracking resistance of asphalt and its mechanical properties such as fracture energy, tensile strength, critical strain energy release, and flexibility index [13]. Moreover, it is also used to characterise the fracture toughness to evaluate the crack resistance and propagation [14,15]. The most recent studies have focused on the long-term effect of freeze–thaw cycles on asphalts [1,6] and the influence of water saturation on fatigue performance [2].

The asphalt's internal structure evolution under freeze–thaw cycles has been previously evaluated using X-ray computed tomography [16,17,18]. This technology allows a micro-scale characterisation to quantify porosity, tortuosity, void circularity, and roundness [17,18]. For example, Özgan and Serin showed an increase of 40% in air void content after 24 days of freeze–thaw cycles [3]. Xu et al. investigated asphalt's internal structure changes under freeze–thaw conditioning using X-ray computed tomography (X-ray CT) technology [9]. Although previous researchers have investigated the influence of freeze–thaw cycles on asphalt degradation, the literature still lacks a comprehensive study on the role of the void's properties and its evolution under freeze–thaw cycles on asphalt performances. Consequently, the water retained in the asphalts varies, causing further modification and property losses. By establishing the correlation between topological changes of voids and mechanical properties losses under freeze–thaw cycles, we will be able to improve our design and prevent damage and failure.

Therefore, the current study seeks to establish a correlation between changes in the mechanical properties of asphalt and changes in the topological properties of voids due to freeze–thaw cycles. This was accomplished by quantifying the mechanical properties of asphalts in dry and wet conditions with a variety of void contents and changes in the internal structure caused by freeze–thaw cycles.

2. Materials and methods

2.1. Specimen preparation

Three asphalt mixture types were manufactured, following BS EN 12697–33 and BS EN 12697–35 [19,20]. Recipes have been selected to represent dense asphalt and a porous asphalt with voids higher and lower than the percolation threshold. All mixtures were compacted to refusal; therefore, the aggregate size and gradation were modified to produce the different air void contents.

Crushed granite aggregates with a maximum size of 20 mm and 60/40 pen bitumen were used for all mixtures. The aggregate gradation and binder contents of asphalts are shown in Table 1. The materials were mixed at 165 ℃ and roller compacted at 165 ℃. Sixteen asphalt slabs of 300 mm × 300 mm × 60 mm were produced with target air voids 3%, 9.8% and, 14%, respectively.

Cylindrical specimens with 100 mm diameter and 60 mm in height were extracted from slabs. The specimens were trimmed by 10 mm on the top and 10 mm on the bottom of the cores using a core saw. 80 cores of 100 mm diameter and 40 mm height were extracted, five cores per slab.

Moreover, two semi-circular specimens were obtained from each core by cutting them along their diameter. A vertical notch of 10 mm with a tolerance of ± 1 mm was introduced along the symmetrical axis with a thickness of 4 ± 0.5 mm to investigate fracture properties.

2.2. Freeze-thaw cycles test method

See the scheme of the tests to investigate the mechanical and cracking resistance properties of asphalts under freeze–thaw cycles in Fig. 1.

The samples were tested in dry and wet conditions. In wet

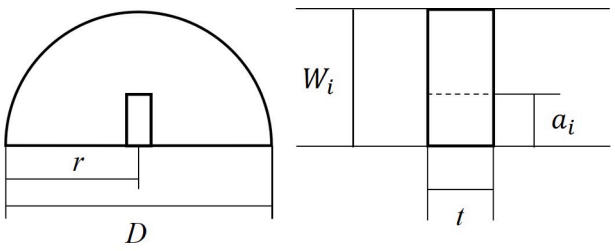

Fig. 3. Semi-circular asphalt specimen dimension.

conditions, the samples were submerged in water at 20 °C for 16 h and then wrapped in a transparent plastic film to keep the water in the samples. After, they were stored at −10 °C for 16 h and then at 20 °C for 8 h for the thawing part of the cycle. In dry conditions, the samples were kept in the air at −10 °C for 16 h and then at 20 °C for 8 h.

The specimens were subjected to up to 20 freeze–thaw cycles. Computed Tomography (CT) scans were taken before and after each cycle to evaluate the topology of void evolution. We CT scanned the same material in a range of cycles; hence, the statistical significance derived from the rate of change of the topological properties of the asphalts. The 3-point bending strength of the samples was measured at −10 °C using an INSTRON (a servo-hydraulic test apparatus) loading frame machine, according to BS EN 12697–44:2019 [21].

2.3. Semi-circular bending test

The semi-circular bending test was used to investigate the fracture properties of asphalt at −10 °C according to BS EN 12697–44 [21]. The parameters measured were peak load, F, young modulus, E fracture toughness, K_i, maximum stress to failure, σ, and fracture energy, G_f.

In this study, semi-circular bending test specimens were tested in a three-point bending load configuration supported by two rollers, with the distance between them 0.8 times the diameter of the semi-circular samples, see Fig. 2.

The load was applied monotonically on top of the specimen at a constant rate of 5 mm/min until material failure occurred and test results were recorded along with the deformation of the specimen (load vs displacement). The peak load at which the specimen fails was also determined.

The maximum stress at failure [21], σ_m, was calculated with:

$$\sigma_m = \frac{4.263xF}{Dxt} \tag{1}$$

where D, t and F are the specimen diameter, m, sample thickness, m of the semi-circular asphalt specimen, and peak load, N, on the sample, see Fig. 3.

The fracture toughness, which describes the material's resistance to fracture, K_i, is calculated as shown in reference [21]:

Table 2
Topology of voids after freeze–thaw cycles, in wet conditions.

Sample (target voids content)	Freeze-thaw Cycle	Air void content (%)	Mean void diameter (mm)	Mean void area (cm^2)	Void perimeter (mm)	Voids Aspect ratio (-)	Voids circularity (-)	Roundness (-)	Euler number	Tortuosity
3%	New	2.96	1.84	603	5.21	1.9	0.72	0.62	1182	0.92
	FT1	3.28	1.67	666	4.85	1.92	0.72	0.61	1358	0.91
	FT2	3.72	1.69	756	4.8	1.94	0.71	0.61	1269	1.30
	FT3	3.23	1.33	656	4.05	1.85	0.75	0.65	1924	1.25
	FT5	3.23	1.33	656	4.05	1.85	0.75	0.65	1967	1.44
	FT20	6.20	1.31	967	5.72	2.01	0.71	0.61	355	0.99
9.8%	New	9.47	4.74	1827	7.9	2.02	0.68	0.6	181	1.43
	FT1	11.48	4.44	2220	7.08	2.06	0.7	0.62	−779	1.69
	FT2	13.34	4.38	2585	7.26	2.13	0.71	0.61	−1304	1.62
	FT3	15.99	4.09	3090	6.76	2.09	0.74	0.63	−2005	1.47
	FT5	15.00	8.90	2900	8.12	2.52	0.64	0.56	−260	1.59
	FT20	14.10	11.62	2757	8.12	2.34	0.66	0.6	−358	1.23
14%	New	13.95	5.40	2927	10.5	2.13	0.59	0.56	−1851	1.58
	FT1	16.16	5.46	3396	10.2	2.09	0.61	0.57	−2248	1.52
	FT2	15.09	5.04	3145	9.53	2.08	0.62	0.58	−1605	1.57
	FT3	16.95	4.48	3539	8.59	2.01	0.66	0.61	−2340	1.47
	FT5	20.56	5.70	4328	10.04	1.99	0.68	0.62	3225	1.35
	FT20	19.78	9.37	4073	11.6	2.17	0.63	0.79	−1871	1.30

FT: freeze–thaw cycles.

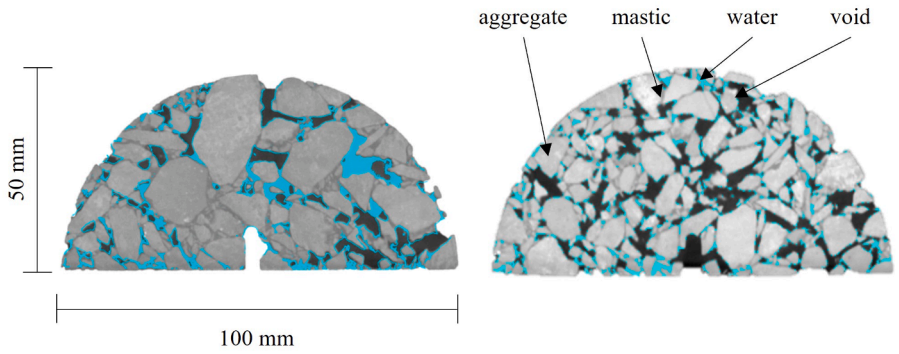

Fig. 4. Example of water retained in the asphalt pores, 9.8% (a) and 14% (b). Blue is described the water retained in the pores, gray is the mastic and aggregates, and black are the voids. (For interpretation of the references to colour in this figure legend, the reader is referred to the web version of this article.)

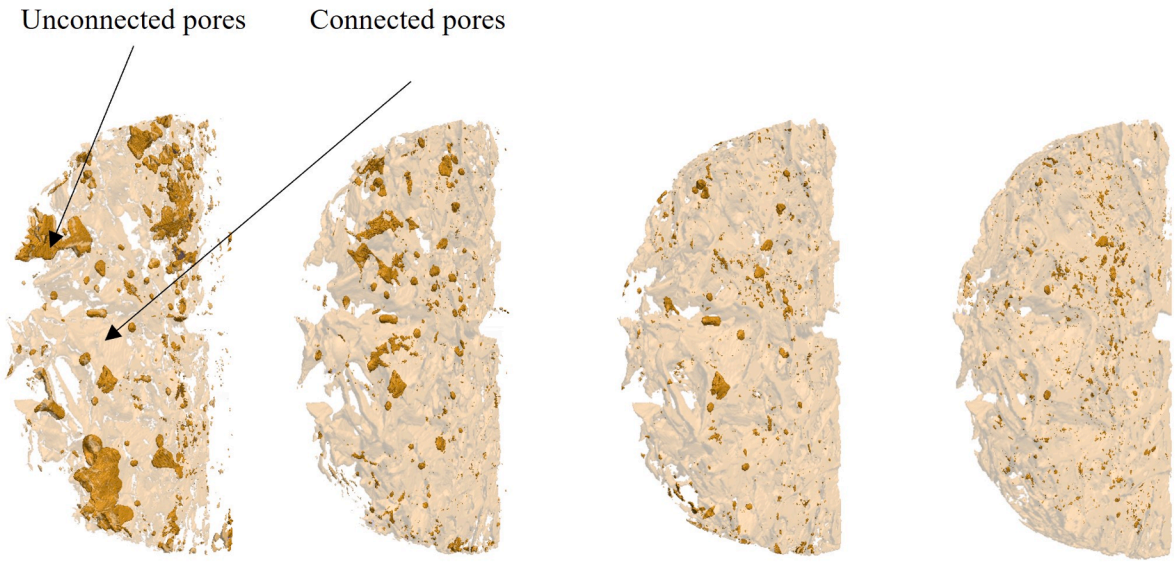

Fig. 5. Evolution of voids with freeze–thaw cycles: Total pores in (a) new (dry) condition and after (b), 1st cycle (c), 2nd cycle (d), 3rd cycle.

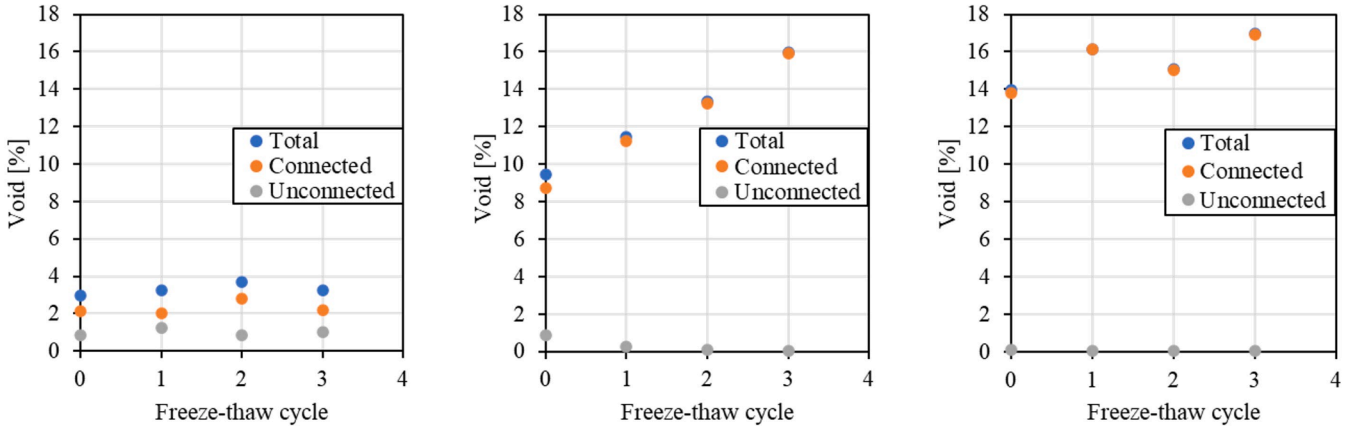

Fig. 6. Void content percentage against freeze–thaw cycles (in wet conditions) for asphalts with target air voids (a) 3%, (b) 9.8%, (c) 14%. Blue points represent the total void content, orange points represent the connected void content, and grey points represent the unconnected void content.

$$K_i = \sigma_m x f(\frac{a_i}{W_i}) \tag{2}$$

where W_i, a_i, and $f(\frac{a_i}{W_i})$ are the height of the specimen, the notch length, both in mm, and a geometric factor, see Fig. 3. The geometric factor $f(\frac{a_i}{W_i})$ is 5.956, for $9 < a_i < 11$ mm and $70 < W_i < 75$ mm. For other a_i and W_i values, the geometric value can be calculated according to the formula presented in reference [21]:

$$f\left(\frac{a_i}{W_i}\right) = -4.9965 + 155.58\left(\frac{a_i}{W_i}\right) - 799.94\left(\frac{a_i}{W_i}\right)^2 + 2141.9\left(\frac{a_i}{W_i}\right)^3 - 2709.1\left(\frac{a_i}{W_i}\right)^4 + 1398.6\left(\frac{a_i}{W_i}\right)^5 \tag{3}$$

The fracture energy [22] is the energy released during cracking, obtained as the area below the load–displacement curve until the specimen is broken following the Equation:

$$G_f = \frac{W}{A_{lig}} \tag{4}$$

Where W and A_{lig} are the work of fracture and the ligament area defined as.

$$A_{lig} = (r - a_i)xt \tag{5}$$

Where, a and t are specimen radius, in m, notch length, in m, and specimen thickness, in m, respectively, see Fig. 3.

2.4. Images acquisition and processing of X-ray CT

The asphalt samples were scanned using a Phoenix v|tome|x L 300 micro CT scanner; the X-ray tube used was (MXR320HP/11, 3.0 mm Be + 2 mm Al from GE Sensing and Inspection Technology) operating with an acceleration voltage of 290 kV and a current of 1300 mA.

The samples were positioned at 906.84 mm from the X-ray source

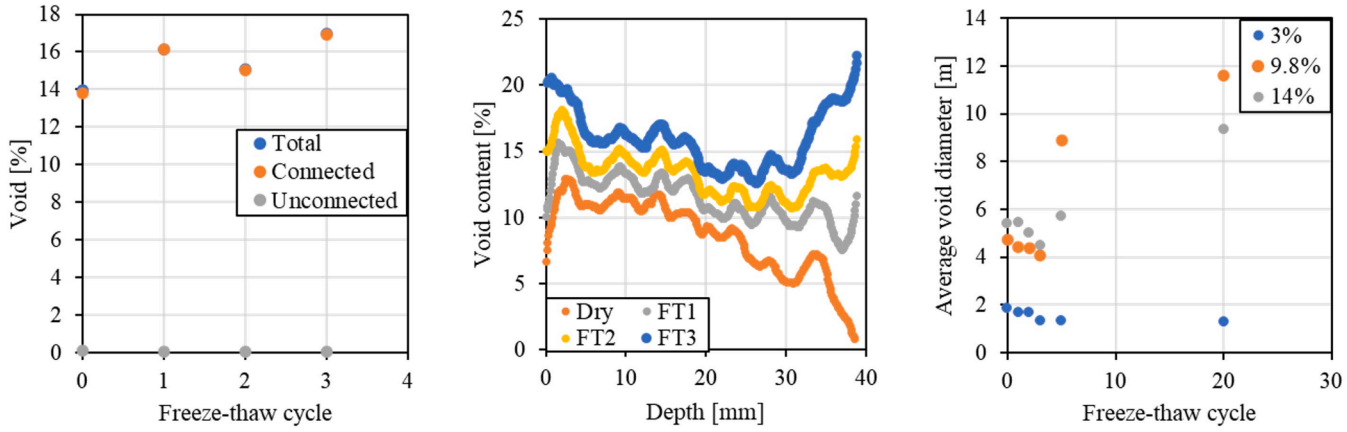

Fig. 7. (a) Average diameter evolution with freeze–thaw cycles. (b) Void content for asphalt with target voids 9.8% against depth. (c) Average void diameter per freeze–thaw cycle.

Table 3
Topology of voids changes rate due to the freeze–thaw cycles.

	Sample (target voids content)	Air void content (% / cycle)	Mean void diameter (mm / cycle)	Mean void area (cm^2 / cycle)	ΔVoids Aspect ratio / cycle	Euler number / cycle	Tortuosity / cycle
Fast damage stage	3%	0.125	−0.151	24.90	−0.013	213.7	0.138
	9.80%	2.142	−0.201	415.50	0.028	−708.3	0.030
	14%	0.793	−0.318	158.50	−0.037	−82.4	−0.028
Slow damage stage	3%	0.158	−0.019	16.34	0.006	−55.8	−0.004
	9.80%	0.111	0.366	23.23	0.013	17.9	−0.017
	14%	0.223	0.220	42.98	0.005	5.9	−0.012

and mounted on a rotational table. The scan images were reconstructed using the GE Datos|x reconstruction software with 2x resolution obtaining a spatial resolution of 45.2 mm; the scans had an isotropic resolution, meaning that the slice thickness was also 45.2 mm.

The original images were in 16-bit (.tiff format), and the voxel value represented the x-ray attenuation, then are processed with the software tools VG studio max and ImageJ, Version 1.8.0 [23,24], and converted to 8-bit grayscale resolution.

The different components of the samples, such as aggregates, mastic, and air voids, were separated by segmenting the materials based on grayscale thresholding using ImageJ. Based on experience, we considered that small isolated clusters with<0.5 mm could be small voids or noise effects and were removed from the image. The segmented images of the air voids were stacked using the software VGSTUDIO MAX, to generate 3D surfaces.

2.5. Density

The test specimens' asphalt mixture density and bulk density were calculated according to BS EN 12697, part 5 [19] and part 6 [19], respectively.

2.6. Air voids content

The air voids content of the samples has been calculated according to Equation (6) [19].

$$V_s = \frac{\rho_m - \rho_b}{\rho_m} \tag{6}$$

where V_s is the air void content of the sample, %, ρ_m is the maximum density of the mixture, kg/m^3, and ρ_b, the bulk density of the test sample, kg/m^3.

2.7. Connected air voids

There are two categories of voids in the asphalt: connected voids and unconnected voids.

Connected voids have at least one end communicating with the external surface and allow water to pass through them. One particular case of connected voids is the dead-end voids with only one end connected to an external surface and retaining water. Unconnected voids do not communicate with the external surface. In this study, we are interested in the connected voids.

The VG studio max software has been used to identify the connected and dead-end voids connected to one of the surfaces.

2.8. Mean void diameter

The mean void diameter, V_{mean}, has been obtained using a thickness algorithm within the Particle Analyser plugin [24] (Version 1.4.3) in Fiji and calculated as:

$$V_{mean} = \frac{\sum_{i=1}^{n} d_i V_i}{\sum_{i=1}^{n} V_i} \tag{7}$$

where, d_i is the diameter of each single void and, V_i is the volume of each pore in the sample.

2.9. Mean void area

The Mean void area is calculated by converting the pores into meshes with triangular shapes and measuring the total surface area of pores and their volume. It was done using the BoneJ surface area [24] plugin (Version 1.4.3). The mean void area is calculated using the Equation:

$$Meanvoidarea = \frac{A}{V} \tag{8}$$

Where A is the total surface of pores and V the volume of the specimen.

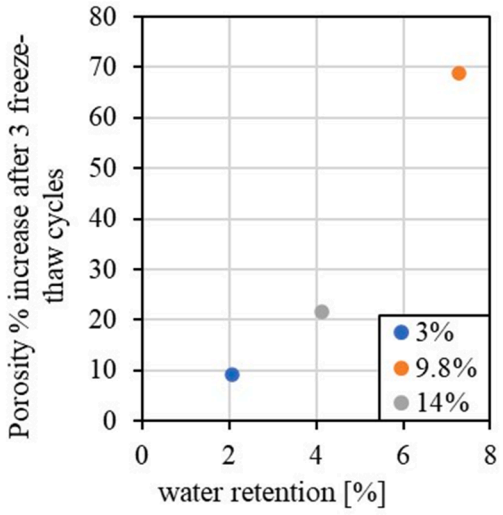

Fig. 8. Water retention [%] at the first cycle versus porosity increase.

2.10. Aspect ratio

The aspect ratio of a void is the ratio between its largest and smallest orthogonal diameters. The aspect ratio's value (A_r) has been obtained using the shape descriptor algorithm within the Particle Analyser plugin [25] (Version 1.4.3) in Fiji and calculated as:

$$A_r = \frac{d_{max}}{d_{min}} \quad (9)$$

Where d_{max} and d_{min} are the largest and smallest orthogonal axis, respectively.

2.11. Circularity

The circularity (*Circ*) has been obtained using the shape descriptors algorithm within the Particle Analyser plugin [25] (Version 1.4.3) in Fiji and calculated as:

$$Circ = \frac{4\pi A}{P^2} \quad (10)$$

Where A is the area and P is the perimeter. A value of 1 means the void is a perfect circle, and a value closer to 0 indicates that the void is elongated.

2.12. Roundness

The roundness measures how similar is the shape of an object to a perfect cycle and it is calculated using the shape descriptors algorithm within the Particle Analyser plugin [25] (Version 1.4.3) in Fiji as:

$$Round = \frac{4A}{\pi {d_{max}}^2} \quad (11)$$

Where A is the area and d_{max} the largest orthogonal axis.

2.13. Tortuosity

Tortuosity, T, is defined as the height of the test specimen to the minimum distance between the two ends of specimen:

$$T = \frac{L_p}{L_s} \quad (12)$$

Where T is the tortuosity, L_p is the total length of pore and, L_s is the shortest distance between the two ends of samples.

The values were obtained with the Skeletonize 2D/3D and Analyse Skeleton modules in ImageJ [25], with no pruning of the dead ends.

2.14. Euler number

The Euler number is the function of the number of isolated air voids, N, the number of redundant connections in air paths, C, and closed cavities, H. A negative Euler number means the air voids are percolated [26,27,28]. These parameters were determined with the BoneJ particle analyser plugin (Version 1.3.11) in ImageJ [25].

$X = N\text{-}C + H$ (13).

3. Results and discussion

3.1. Internal structure evolution of asphalt mixtures during freeze–thaw cycles

Table 2 shows how the topology of voids changes after each freeze–thaw cycle in asphalt that had been previously submerged in water. These values have been obtained from CT-Scans and are the average properties of each CT-Scan. We have selected mixtures with target air voids 3%, 9.8% and 14%, due to their high difference in voids content, which are representative of dense, semi-dense and porous asphalts. Please note that referring to samples as "new" implies that they were tested in dry conditions prior to being frozen and thawed.

Besides, to have a visual idea of how the water is retained in the asphalt, Fig. 4 shows the presence of water in asphalts with 9.8% target air voids and 14% target air voids after they have been submerged and removed from the water. This figure shows that the voids are not full of water, which is retained only in the dead-end voids and the narrowest areas.

The voids in asphalt can be connected or unconnected [29]. They are unconnected when they do not communicate with the atmosphere and connected when they communicate. According to previous studies [30], connected pores are the only types that allow water to penetrate through the asphalt during freeze–thaw cycles. Therefore, in this study, we identified the connected and unconnected pores to determine their influence on the effect of freeze–thaw cycles on asphalt's durability. Fig. 5 (a) illustrates the asphalt's connected and unconnected air voids, with a target air void percentage of 9.8%. Before the specimen was subjected to freeze–thaw cycles, the mixture had 8.7% connected voids and 0.86% unconnected voids. After three freeze–thaw cycles, the mixture had 15.9% connected voids and 0.05% unconnected voids. With every cycle, the asphalt became more porous, which increased the amount of water damage with each freeze–thaw cycle.

Moreover, Fig. 5 shows the void content evolution with the freeze–thaw cycles of the three types of asphalt studied, highlighting the connected and unconnected voids since that may help understand their evolution with the number of freeze–thaw cycles. With the freeze–thaw cycles, the total voids and the connected voids increased in every asphalt studied, and the unconnected voids decreased. The unconnected voids in the mixture with target air voids 3% remained approximately stable during the freeze–thaw cycles, while the connected voids increased from approximately 2.12% to 2.8%. For the mixture with target air voids 9.8%, the total voids content increased from 9.5% to 14.1%, which are 48% more. Furthermore, the unconnected voids reduced from 0.86% to 0.05%, and the connected voids increased from 8.7% to 15.9% in three freeze–thaw cycles, a growth of 83%. In addition, in the mixture with 14.0% void content, the connected porosity increased up to 16.9%, a growth of 22%.

In reference [30], the authors divided the evolution of voids during freeze–thaw cycles into three arbitrary stages (i) initial stage, (ii) steady increase stage and (iii) increase stage; however, in this paper, it is unclear what each of these stages means and, the number of cycles in each stage varied depending on the type of asphalt mixtures. Moreover, in [6], the stiffness of the asphalt they studied reduced steadily until approximately the 5th freeze–thaw cycle and after, the stiffness

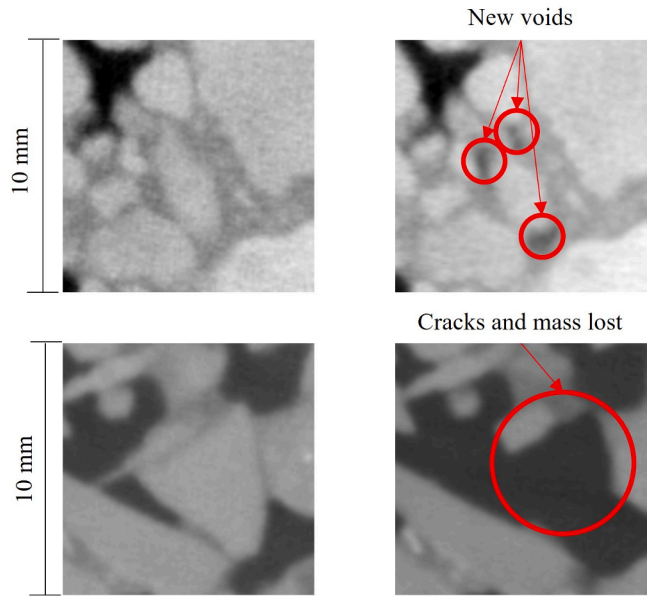

Fig. 9. CT scan of new asphalt and damaged after 20 cycles. (a) Asphalt with target voids 9.8% before the freeze–thaw cycles. (b) Asphalt with target voids 9.8% after 5 cycles. (c) Asphalt with target voids 14% before the freeze–thaw cycles. (d) Asphalt with target voids 14% after 20 cycles.

remained steady with additional freeze–thaw cycles. Hence, the authors have tested the evolution of voids in asphalts for 20 freeze–thaw cycles and, based on observation, decided to divide the freeze–thaw cycles into two stages: (i) fast damage stage and (ii) slow damage stage.

In Table 3, we describe the rate of change of topological properties of the asphalts, ranging from 0 to 3 cycles, to describe the fast damage stage and from 0 to 20 cycles to describe the slow damage stage. We have used Fig. 7 (a), which shows the evolution of air voids for the three types of asphalt analysed with the number of freeze–thaw cycles, to select the range of freeze–thaw cycles for the fast and the slow damage stages.

The first remarkable aspect observed in Table 3 and Fig. 7 (a) is that the air voids content increased for every asphalt studied during the freeze–thaw cycles. The average rate of air voids increase was 1.02%/cycle in the fast damage stage and 0.16 %/cycle in the slow damage stage. In general, it can be observed that the voids increase linearly with the freeze–thaw cycles at a rate of 0.12 %/cycle for the asphalt with target voids of 3%, 2.14 %/cycle for the asphalt with target voids of 9.8% and 0.79 %/cycle for the asphalt with target voids 14%. The asphalt with a target air void of 9.8% suffers greater damage than the rest of the test samples during the fast damage stage [32]. Besides, Fig. 7 (b) shows how the voids change with the depth of the specimen (thickness, which is the *t* dimension in Fig. 3) in asphalt with 9.8% voids content. This mixture had segregation, as seen in the connected voids that reduced with the height. However, the voids increased and became progressively connected with the cycles, which gives an idea of how the asphalt gets damaged due to freeze–thaw cycles under wet conditions.

To explain the higher increase of porosity in the mixture with target air voids 9.8%, Fig. 8 correlates the increase in porosity with the water retained in the three asphalts studied. We found using the CT scans that the percentages of water retained by weight of the asphalts are 2.05%, 7.28%, and 4.13% for the mixtures with 3%, 9.8%, and 14% target voids, respectively. Hence, there is a linear relationship between the amount of water retained in the asphalt and the physical damage it suffers in each freeze–thaw cycle, suggesting that to minimise the freeze–thaw damage, the internal structure of the pores plays a key role.

As a result of the higher water retention rate, asphalt with 9.8% target voids has the highest increase of porosity and area in the fast damage stage, see Table 3, which is similar to the results reported in [10]. However, in this mixture, the diameter of the voids decreased, which indicates the creation of several small pores or cracks with a small diameter. Besides, it is interesting that the mixture with target voids of 3% had the lowest rate of void diameter increase, which, as can be observed in Table 3, must be related to having the lowest water retention rate. In general, in Table 3, we can observe that during the fast damage stage, the void diameter decreased for all the asphalts analysed, which could indicate the creation of new voids and cracks in the material, which were smaller than the existing voids; for example, see examples in Fig. 9 (a) and Fig. 9 (b), for the asphalt with 9.8 target voids content.

In the slow damage stage, after the third freeze–thaw cycle, cracks widened, which caused some aggregates to fall through the voids; see Fig. 9 (c) and (d) for an example. In this stage, the voids area increased for the three mixtures studied, and the tortuosity decreased steadily, which could be due to voids coalescing and creating bigger voids, as explained in reference [10]. For example, for the mixture with a target air void of 3%, in 20 cycles, the voids increased steadily from 2.96% to 6.2%, and the Euler number and tortuosity decreased, reflecting that the pores were better connected, and cracks started to appear. It is expected that when the voids topologies of the mixture with target air void 3% become like those of mixture with target air void 9.8%, more water will be retained, and there will be a sudden increase of damage, which may explain why some dense asphalts that have been several years in service get suddenly damaged after a cold day. This has been reported before in reference [6], where the asphalts resist several freeze–thaw cycles until they break suddenly.

Furthermore, from Table 3, it is apparent that the initial aspect ratio of the voids in all the asphalts studied is greater than 1, implying that the voids are not circular; with each freeze–thaw cycle, the aspect ratio decreases and the voids become circular. If the aspect ratio increases, it can be inferred that cracks are more prevalent than new pores, which would be reflected by a negative increase in the asphalt ratio. The rate of growth of the aspect ratio for the mixture with 9.8% voids content is positive. Hence, during the fast damage stage, the formation of cracks is predominant in this mixture. Also, see how the Euler number decreases, meaning more connectivity in the pores. In the other two mixtures, the voids became rounder, reflecting the formation of new small unconnected voids in the asphalt. Finally, the aspect ratio increased steadily with the cycles in the slow damage stage, which implies that the cracks grew gradually.

We analysed the R^2 values of topological properties from Table 2 versus the number of cycles in wet conditions to confirm the results. A R^2 value of 1 indicates a direct correlation between two variables, while a

Table 4
R^2 values of the void's topological values versus the freeze–thaw cycles in wet conditions.

	Sample (target voids content)	Air void content	Mean void diameter	Mean void area	ΔVoids Aspect ratio	Euler number	Tortuosity
Fast damage stage	3%	0.263	0.819	0.256	0.189	0.678	0.727
	9.80%	0.994	0.948	0.995	0.603	0.986	0.003
	14%	0.616	0.832	0.570	0.916	0.096	0.509
Slow damage stage	3%	0.927	0.401	0.845	0.464	0.466	0.012
	9.80%	0.136	0.801	0.154	0.300	0.035	0.594
	14%	0.460	0.894	0.404	0.219	0.000	0.684

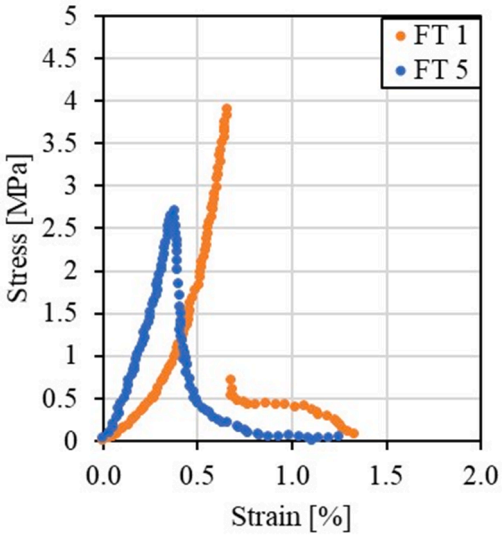

Fig. 10. Examples of stress–strain curves for the asphalt with 9.8% air voids content.

R^2 value of 0 indicates no correlation between the variables. In the fast damage stage for semi-open and open asphalts, the R^2 value is close to 1 for most properties, indicating a clear trend of change with the freeze–thaw cycles and confirming that damage occurs in this stage for these two types of asphalt. Moreover, in the slow damage stage, the topologies of dense asphalt strongly correlated with the number of cycles, confirming that dense asphalt degraded slowly with the cycles in wet conditions. However, semi-dense and porous asphalt showed lower correlations, which confirms that most of the damage in these materials occurred during the fast damage stage, as shown in Fig. 6. Furthermore, the authors appreciate that the Euler number and tortuosity may change with the number of cycles, as it was mentioned above; however, one cannot appreciate a clear trend in the data shown in Table 4.

3.2. *Effect of freeze–thaw cycles on the asphalt's mechanical properties*

An example of the semi-circular bending test results of asphalt with 9.8% of void content is shown in Fig. 10. The stress–strain curve followed a brittle behaviour; the load increased with compression with a brittle and sudden fracture after the load reached the peak force, exceeding the bearing capacity of the material.

Fig. 11 shows the evolution of various mechanical properties such as peak load, see Fig. 11(a), Young modulus, Fig. 11(b), fracture toughness, Fig. 11(c), and fracture energy, Fig. 11(d), with the freeze–thaw cycles. The four mechanical properties reflect the fast and slow damage stages that we mentioned above, where the mechanical properties degrade with the first five cycles; in this case, it can be seen that the fast damage stage lasts between 3 and 5 cycles, while the damage growth rate is reduced in the slow damage phase, as expected [32]. Moreover, in Table 5, the data from Fig. 11 have been presented to allow easy comparison to the topological values from Table 2. As established in Table 3, the reduction rate depended on the initial internal structure of asphalt.

As seen in Fig. 9, with the increase in freeze–thaw cycles, new voids are created, cracks are formed, and aggregates are lost in the voids, which increases the connected voids [9]. Moreover, increased air-voids content provides space for frost heaving generated by subsequent freeze–thaw cycles and slows the damage growth, as seen in Table 3. A similar reduction of mechanical properties was presented in [1,5,31], with an initial reduction of fracture toughness and a plateau after the fifth cycle. Furthermore, in [12], the Young modulus and fracture toughness dropped about 30% after one freeze–thaw cycle and slowly reduced.

In previous studies, it was found that asphalts with porosity ranging from 6% to 13% have, in general, lower durability than other asphalts [2,3,5,6,9]; in general, most of these studies did not consider the topology of pores in the asphalt and the changes that occur to these voids in the freeze–thaw cycles. As shown in Table 2 and Fig. 8, the asphalt with 3% air void content is characterised by having the smallest void diameter, highest Euler number, and lowest water retention rate. The asphalt with 9.8% air void content has an intermediate voids diameter, Euler number and the highest water retention rate. Finally, the asphalt with 14% of air voids has the highest voids diameter, smallest Euler number and an intermediate water retention rate. The authors found linear correlations between the mechanical and some of the topological properties of the pores at the range of freeze–thaw cycles studied. The Pearson correlations have been presented in Table 6.

Reference [29] shows a strong and direct positive correlation between the air voids content, voids diameter or perimeter and volume of the biggest air void and Euler number. Hence, we refer to these properties by referring to the air void content. In Table 6, we observe a strong negative correlation between the air void content and the peak load, Young modulus, and fracture toughness of the asphalts. During the fast-damage stage, all of these properties declined with increasing air void content regardless of the gradation, asphalt composition, or previous freeze–thaw cycles. Based on this, it could be possible to approximately predict the freeze–thaw durability of asphalt by simply measuring its voids content, and one can conclude that the main source of low durability for the asphalt during the freeze–thaw cycles is the physical damage it suffers from increasing its voids size and content. Moreover, despite the high reduction rate in the fast damage stage, the mechanical properties did not undertake additional damage, reaching a steady stage, which indicates that asphalt with higher void content has the highest long-term durability. The tortuosity influences also the mechanical properties indicating that asphalt with more twisty void shapes, with lower circularity and higher aspect ratio, has lower ultimate strength, fracture toughness and fracture energy. Finally, the fracture energy shows the same trend as the rest of the mechanical properties studies; however, it does not seem to be strongly correlated to any of the topological properties being considered, which may occur because this property is related to the mastic properties rather than to the asphalt's gradation.

Besides, Fig. 12 shows the slope of the percentage reduction of peak load, young modulus, fracture toughness and fracture energy during the first three freeze–thaw cycles. This figure shows the asphalt that reduced its mechanical properties most due to freeze–thaw, regardless of the initial strength of the material.

The peak load, fracture toughness and fracture energy of asphalt with target air voids content of 9.8% reduced the most; the Young modulus, defined as the relationship between the peak load and the deformation at the peak load, did not reduce as much as in the other two materials, probably because the asphalts broke before the deformation could reach a high value. From Table 2, it can be observed that the topological properties of air voids in the asphalt with target voids of 9.8% are not higher than those of the asphalt with target air voids of 14%. The only difference between both asphalts was the water retained, which was 2.05%, 7.28% and 4.13% by total weight in the mixtures with target air voids of 3%, 9.8% and 14%, respectively. Hence, one can conclude that the capacity to retain water by the asphalts is a key factor regarding its durability to freeze–thaw cycles.

Fig. 13 displays the fracture toughness reduction rate per cycle for all samples in dry and wet conditions after three cycles. The result shows that the asphalt tested in wet conditions has the highest strength reduction within three cycles; hence, this figure demonstrates the damage caused by water to the asphalt during the freeze–thaw cycles. Interestingly, in dry conditions, the asphalt with target air voids of 3% suffers the greatest damage, possibly due to the highest amount of bitumen, which has a different coefficient of thermal expansion compared to the aggregates. Aggregates and bitumen contract and

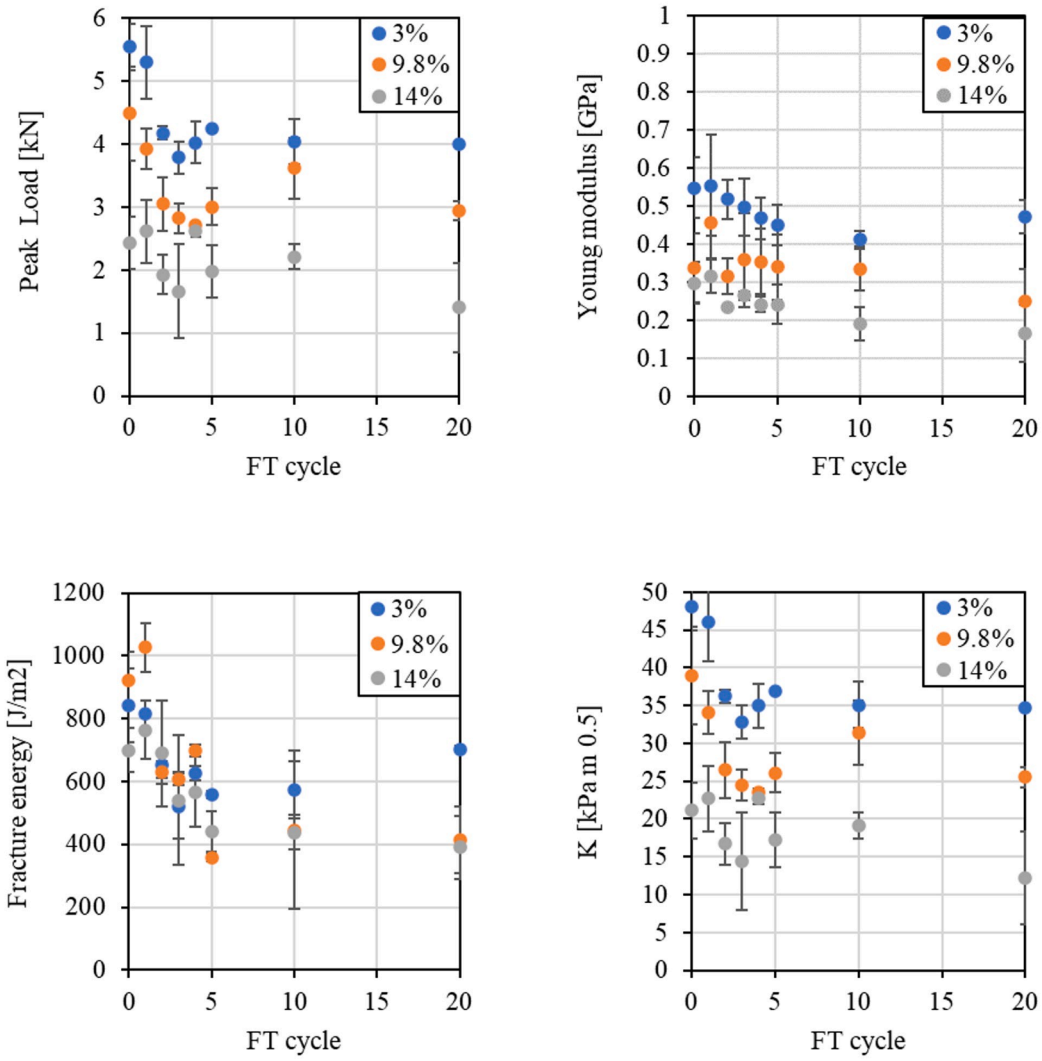

Fig. 11. Evolution of (a) Peak load, (b) Young modulus, (c) Fracture toughness, (d) Fracture energy with the freeze–thaw cycles.

Table 5
Mechanical properties of the test samples examined.

Sample (target voids content)	Values Freeze Cycle	Peak load (kN)	Young Modulus (GPa)	Fracture toughness (kPa m 0.5)	Fracture energy (J/m^2)	Standard deviation Peak load (kN)	Young Modulus (GPa)	Fracture toughness (kPa m $^{0.5}$)	Fracture energy (J/m^2)
3%	New	5.54	0.55	841	48.14	0.37	0.08	117	3.23
	FT1	5.29	0.56	814	45.97	0.58	0.13	246	5.05
	FT2	4.17	0.52	651	36.23	0.10	0.05	39	0.90
	FT3	3.78	0.50	521	32.84	0.25	0.07	104	2.17
	FT5	4.25	0.45	558	36.92	0.01	0.05	11	0.07
	FT20	4.00	0.47	704	34.76	0.02	0.05	10	0.07
9.8%	New	4.48	0.34	921	38.93	0.74	0.09	91	6.43
	FT1	3.92	0.46	1027	34.03	0.32	0.10	77	2.80
	FT2	3.05	0.32	628	26.46	0.42	0.05	37	3.67
	FT3	2.82	0.36	609	24.53	0.24	0.12	21	2.07
	FT5	3.00	0.34	359	26.09	0.30	0.09	12	2.58
	FT20	2.94	0.25	414	25.54	0.15	0.08	107	1.34
14%	New	2.43	0.30	699	21.11	0.42	0.05	70	3.67
	FT1	2.61	0.32	763	22.70	0.50	0.05	93	4.30
	FT2	1.93	0.23	689	16.77	0.32	0.00	168	2.75
	FT3	1.67	0.27	540	14.47	0.74	0.01	206	6.47
	FT5	1.99	0.24	440	17.25	0.42	0.05	64	3.61
	FT20	1.40	0.17	390	12.19	0.71	0.07	101	6.17

Table 6
Pearson correlations between the samples' mechanical and topological properties, including new asphalt (dry condition) and, after going through freeze–thaw cycles.

	Air void content	Average void diameter	Volume of biggest air void	Void perimeter (%)	Voids Aspect ratio (%)	Voids circularity (%)	Euler	Tortuosity
Peak load (kN)	−0.89	−0.61	−0.90	−0.81	−0.45	0.64	0.77	−0.55
Young Modulus (GPa)	−0.91	−0.78	−0.91	−0.89	−0.55	0.70	0.75	−0.51
Fracture toughness (kPa $m^{0.5}$)	−0.89	−0.61	−0.90	−0.81	−0.45	0.64	0.77	−0.55
Fracture energy (J/m^2)	−0.40	−0.50	−0.40	−0.24	−0.43	0.14	0.08	−0.04

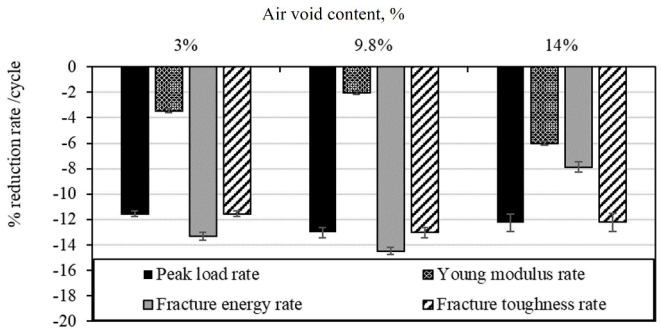

Fig. 12. Percentage of reduction per cycle for the: (a) Peak load, (b) Young modulus, (c) fracture toughness, and (d) fracture energy.

expand differently during the freeze–thaw cycles, causing stress during the freeze–thaw cycles. The results align with references [33,34]. These

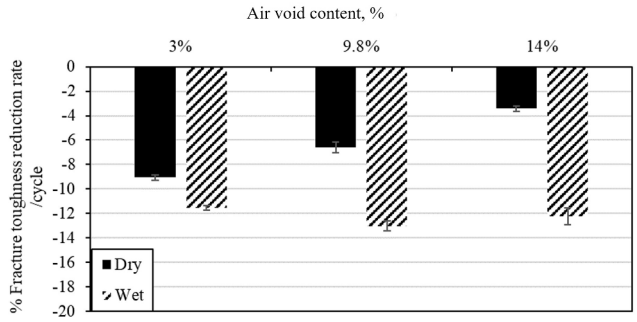

Fig. 13. Percentage of fracture toughness reduction per cycle for dry and wet conditions.

authors observed a drop in mechanical properties for asphalt with air void content of around 3%, concluding that the principal factors influencing degradation are bitumen content and aggregate type and shapes..

3.3. Summary

Fig. 14 shows how the damage progresses for the three types of asphalt analysed in the slow and fast damage stages.

In the asphalt with target air voids 3%, the connected voids increased gradually during the slow and fast damage phases, see Fig. 14 (a). During the slow damage phase, the unconnected voids content remained approximately stable, and the connected voids content increased gradually. As a result, the fracture toughness, fracture energy, Young modulus and peak load of the asphalt decreased [9]. This was the asphalt that retained less water, and hence, it was characterised by high fracture energy and resistance to low-temperature cracking. However, in dry conditions, this asphalt is the one that degrades the fastest.

In the asphalt with target air voids of 9.8%, the voids content grew approximately 48% in 20 cycles; the unconnected voids reduced to approximately none, while all the rest of the voids were connected, see Fig. 14 (b). This mixture retained the most water because it had a high content of open voids with one closed end. As a result, several cracks appeared, very fast during the fast damage phase and progressively during the slow damage phase [10,30]; these cracks coalesced to the extent that aggregates were lost. This resulted in the largest decrease in mechanical properties among all the asphalts studied [6].

Finally, the asphalt with target air voids of 14% retained less water than the previous one, and the ice had more room to expand; hence, the reduction in mechanical properties was lower [30]. The voids in this asphalt were mostly connected and increased their size and total air voids content with the freeze–thaw cycles. In dry conditions, this is the asphalt that degrades more slowly.

4. Conclusions

Several types of asphalt with acceptable air void contents ranging from 3% to 14% were examined for their influence during freeze–thaw cycles, where a correlation between differences in air void topology and changes in mechanical properties was established. According to the results in this study, the topological properties evolution under freeze–thaw cycles was influenced by three different phenomena: (1) volume increase of the existing voids and formation of small cracks, (2) voids coalescence, and (3) cracking and new voids formation. The voids were analysed using X-ray CT scans after every freeze–thaw cycle, and the mechanical properties were measured from 3-point bending tests. The following conclusions were obtained:

The three different asphalts had different behaviours when exposed to freeze–thaw cycles, attributed to the different aggregate size distributions and air void topologies. Hence, the durability of asphalt to freeze–thaw cycles could be controlled by carefully selecting the aggregate gradation, aggregate morphology and air void topologies.

The damage under wet conditions progressed in two stages; (i) fast damage stage and (ii) slow damage stage. The fast damage stage lasted approximately three freeze–thaw cycles and new voids and cracks formed rapidly; the peak load strength reduced fast too. The slow damage stage occurred after the fast damage stage, and the voids and cracks opened gradually. Therefore, the mechanical properties reduced gradually too.

In wet conditions, the asphalt with target air voids of 9.8% showed the highest level of damage in the fast damage stage and the lowest in the slow damage stage. The reason was that this asphalt retained the highest amount of water in the pores of all the three types studied. Water retention and air void content were among the main parameters influencing the durability of asphalt; hence, the durability of asphalt can be controlled with the gradation and mastic content. This result suggests that open grade asphalt may perform best in cold regions.

In wet conditions, the fast damage stage could not be appreciated in the asphalt with target air voids of 3%; the reason was that the voids in this mixture were not connected, and the water retained was minimal. Hence, damage progressed slowly and constantly in this asphalt, leading to sudden failure. The fast damage stage occurred in the mixtures where voids were connected, and the water retention by weight of the asphalt was high.

Unlike in wet conditions, in dry conditions, the asphalt with target air voids of 3% suffered the highest amount of damage during the

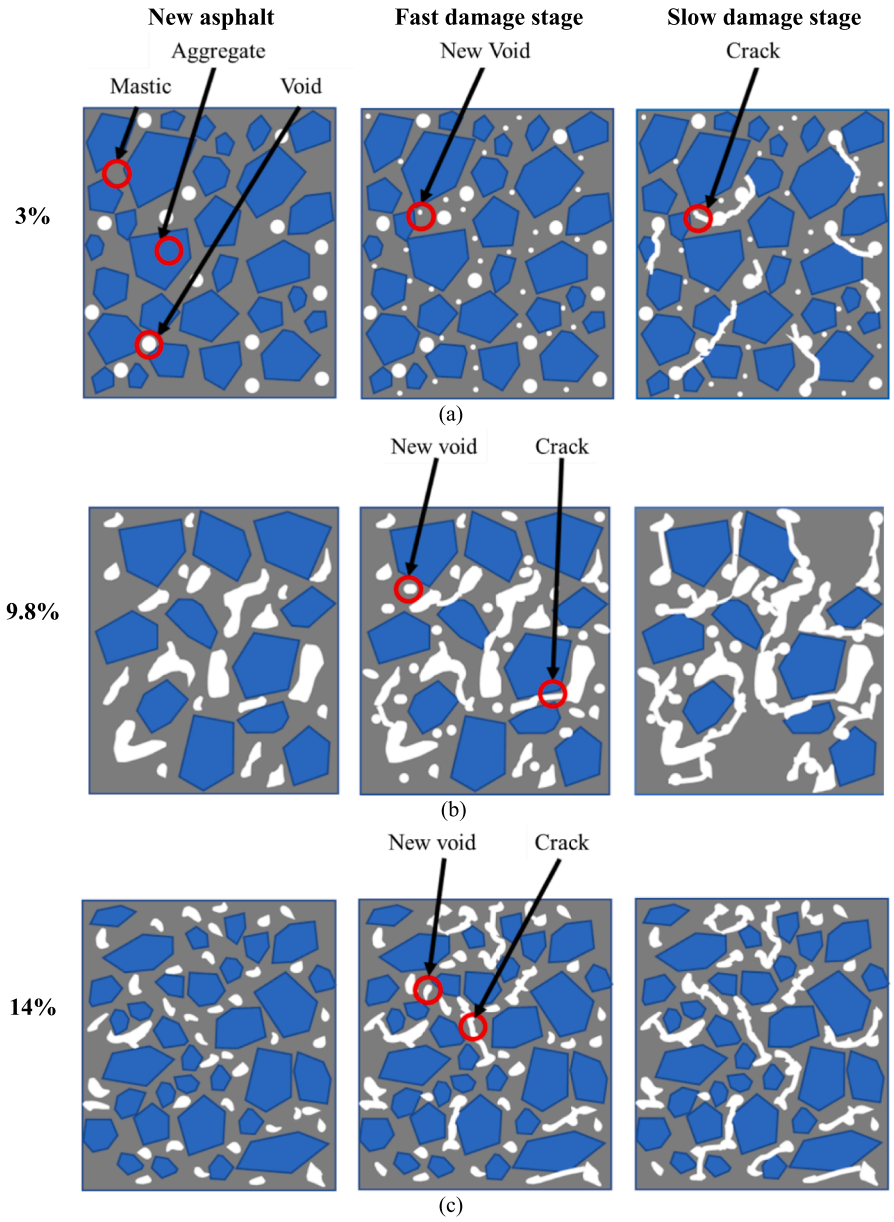

Fig. 14. (a) schematic representation of the three sample during the two stages: (a) 3%; (b) 9.8%; (c) 14%.

freeze–thaw cycles due to the higher amount of aggregates and bitumen and their thermal expansion.

Based on these findings, we can conclude that the internal void topology influences the mechanical properties of asphalt through freeze–thaw cycles; and that open grade asphalt may perform well in cold climates.

The initial water retention of the asphalt could be established as the index to determine the durability of the asphalt, with equal importance to measuring the air voids and macrotexture, as it is done at present.

Declaration of Competing Interest

The authors declare that they have no known competing financial interests or personal relationships that could have appeared to influence the work reported in this paper.

Acknowledgements

The first author acknowledges the funding of the Universities of Nottingham and Birmingham for the stipend and National Highways for the funding for experiments.

References

[1] M.M. Karimi, E.A. Dehaghi, A. Behnood, A fracture-based approach to characterise long-term performance of asphalt mixes under moisture and freeze-thaw conditions, Eng. Fract. Mech. 241 (2021), 107418.
[2] Z. Fan, H. Xu, J. Xiao, Y. Tan, Effects of freeze-thaw cycles on fatigue performance of asphalt mixture and development of fatigue-freeze-thaw (FFT) uniform equation, Constr. Build. Mater. 242 (2020), 118043.
[3] E. Özgan, S. Serin, Investigation of certain engineering characteristics of asphalt concrete exposed to freeze-thaw cycles, Cold Reg. Sci. Technol. 85 (2013) 131–136.
[4] S. Wu, R. He, H. Chen, Y. Luo, Low temperature characteristics of asphalt mixture based on the semi-circular bend and thermal stress restrained specimen test in alpine cold regions, Constr. Build. Mater. 311 (2021), 125300.
[5] M. Fakhri, S. Ali Siyadati, M.R.M. Aliha, Impact of freeze–thaw cycles on low temperature mixed mode I/II cracking properties of water saturated hot mix asphalt: An experimental study, Constr. Build. Mater. 261 (2020) 119939.
[6] M. Sol-Sánchez, F. Moreno-Navarro, G. García-Travé, M.C. Rubio-Gámez, Laboratory study of the long-term climatic deterioration of asphalt mixtures, Constr. Build. Mater. 88 (2015) 32–40.

[7] J. Yi, S. Shen, B. Muhunthan, D. Feng, Viscoelastic-plastic damage model for porous asphalt mixtures: Application to uniaxial compression and freeze-thaw damage, Mech. Mater. 70 (2014) 67–75.
[8] S. Badeli, A. Carter, G. Doré, Complex Modulus and Fatigue Analysis of Asphalt Mix after Daily Rapid Freeze-Thaw Cycles, J. Mater. Civ. Eng. 30 (2018) 04018056.
[9] L. Cong, M. Ren, J. Shi, F. Yang, G. Guo, Experimental investigation on performance deterioration of asphalt mixture under freeze–thaw cycles, Int. J. Transp. Sci. Technol. 9 (3) (2020) 218–228.
[10] H. Xu, W. Guo, Y. Tan, Internal structure evolution of asphalt mixtures during freeze-thaw cycles, Mater. Des. 86 (2015) 436–446.
[11] Y. Cheng, D.i. Yu, G. Tan, C. Zhu, Low-temperature performance and damage constitutive model of eco-friendly basalt fiber-diatomite-modified asphalt mixture under freeze-thaw cycles, Materials (Basel) 11 (11) (2018) 2148.
[12] J. Li, F. Wang, F.u. Yi, J. Ma, Z. Lin, Fractal analysis of the fracture evolution of freeze-thaw damage to asphalt concrete, Materials (Basel). 12 (14) (2019) 2288.
[13] C. Zhang, H. Wang, X.u. Yang, Low-temperature performance of SBS modified asphalt mixture in high altitude and cold regions, Int. J. Pavement Res. Technol. 12 (1) (2019) 33–42.
[14] G. Saha, K.P. Biligiri, Fracture properties of asphalt mixtures using semi-circular bending test: A state-of-the-art review and future research, Constr. Build. Mater. 105 (2016) 103–112.
[15] J. Ren, L. Sun, Characterising air void effect on fracture of asphalt concrete at low-temperature using discrete element method, Eng. Fract. Mech. 170 (2017) 23–43.
[16] S. Pirmohammad, A. Kiani, Study on fracture behaviour of HMA mixtures under mixed mode I/III loading, Eng. Fract. Mech. 153 (2016) 80–90.
[17] E. Masad, V.K. Jandhyala, N. Dasgupta, N. Somadevan, N. Shashidhar, Characterisation of air void distribution in asphalt mixes using X-ray computed tomography, J. Mater. Civ. Eng. 14 (2002) 122–129.
[18] M.E. Kutay, Modeling Moisture Transport in Asphalt Pavements(Ph.D Thesis), University of Maryland, College Park, US, 2005.
[19] N. Abdul Hassan, G.D. Airey, N.I. Nur, M.R. Hainin, R. Putrajaya, M.E. Abdullah, M.M.A. Aziz, Microstructural characterisation of dry mixed rubberised asphalt mixtures, Constr. Build. Mater. 82 (2015) 173–183.
[20] EN 12697-22. (2020). BSI Standards Publication - Bituminous mixtures - Test methods, Part 22: Wheel tracking.
[21] BSI Standards Publication Bituminous mixtures — Material specifications Part 5 : Stone Mastic Asphalt, BSI Br. Stand. (2016).
[22] BS EN 12697-44-2010–[2021-10-25–06-49-03 PM].pdf, (n.d.).
[23] AASHTO, Standard method of test for determining the fracture energy of asphalt mixtures using the semi-circular bend geometry (SCB), Des. TP105 − 13. (2013) 1–14.
[24] G. Volume Graphics, VGStudio MAX 3.0. Reference Manual, 2016.
[25] M.D. Abramoff, P.J. Magalhaes, S.J. Ram, Image processing with ImageJ. Biophotonics Int 11 (7) (2004) 36–42.
[26] M. Doube, M.M. Kłosowski, I. Arganda-Carreras, F.P. Cordelieres, R.P. Dougherty, J.S. Jackson, B. Schmid, J.R. Hutchinson, S.J. Shefelbine, BoneJ: free and extensible bone image analysis in ImageJ, Bone 47 (6) (2010) 1076–1079.
[27] H.J. Vogel, Morphological determination of pore connectivity as a function of pore size using serial sections, Eur. J. Soil Sci. 48 (1997) 365–377.
[28] H.-J. Vogel, K. Roth, Quantitative morphology and network representation of soil pore structure, Adv. Water Resour. 24 (3-4) (2001) 233–242.
[29] M. Aboufoul, A. Garcia, Factors affecting hydraulic conductivity of asphalt mixture, Mater. Struct. Constr. 50 (2) (2017).
[30] Z. Zhang, Q. Liu, Q. Wu, H. Xu, P. Liu, M. Oeser, Damage evolution of asphalt mixture under freeze-thaw cyclic loading from a mechanical perspective, Int. J. Fatigue. 142 (2021) 1–9.
[31] D. Feng, J. Yi, D. Wang, L. Chen, Impact of salt and freeze-thaw cycles on performance of asphalt mixtures in coastal frozen region of China, Cold Reg. Sci. Technol. 62 (1) (2010) 34–41.
[32] G. Xu, Y. Yu, D. Cai, G. Xie, X. Chen, J. Yang, Multi-scale damage characterisation of asphalt mixture subject to freeze-thaw cycles, Constr. Build. Mater. 240 (2020), 117947.
[33] H.M. El Hussein, A.O.A. El Halim, Differential thermal expansion and contraction: a mechanistic approach to adhesion in asphalt concrete, Can. J. Civ. Eng. 20 (1993) 366–373.
[34] D. Jung, T.S. Vinson, Thermal stress restrained specimen test to evaluate low-temperature cracking of asphalt-aggregate mixtures, Transp. Res. Rec. 12–20 (1993).